

## Modeling Electronic Circular Dichroism within the Polarizable Embedding Approach

Nørby, Morten; Olsen, Jógvan Magnus Haugaard; Svendsen, Casper Steinmann; Kongsted, Jacob

*Published in:*  
Journal of Chemical Theory and Computation

*DOI (link to publication from Publisher):*  
[10.1021/acs.jctc.7b00712](https://doi.org/10.1021/acs.jctc.7b00712)

*Publication date:*  
2017

*Document Version*  
Early version, also known as pre-print

[Link to publication from Aalborg University](#)

*Citation for published version (APA):*  
Nørby, M., Olsen, J. M. H., Svendsen, C. S., & Kongsted, J. (2017). Modeling Electronic Circular Dichroism within the Polarizable Embedding Approach. *Journal of Chemical Theory and Computation*, 13(9), 4442-4451. <https://doi.org/10.1021/acs.jctc.7b00712>

### General rights

Copyright and moral rights for the publications made accessible in the public portal are retained by the authors and/or other copyright owners and it is a condition of accessing publications that users recognise and abide by the legal requirements associated with these rights.

- Users may download and print one copy of any publication from the public portal for the purpose of private study or research.
- You may not further distribute the material or use it for any profit-making activity or commercial gain
- You may freely distribute the URL identifying the publication in the public portal -

### Take down policy

If you believe that this document breaches copyright please contact us at [vbn@aub.aau.dk](mailto:vbn@aub.aau.dk) providing details, and we will remove access to the work immediately and investigate your claim.

# Modeling electronic circular dichroism within the polarizable embedding approach

Morten S. Nørby,<sup>\*,†</sup> Jógvan Magnus Haugaard Olsen,<sup>†</sup> Casper Steinmann,<sup>‡</sup> and  
Jacob Kongsted<sup>†</sup>

<sup>†</sup>*Department of Physics, Chemistry and Pharmacy, University of Southern Denmark,  
DK-5230 Odense M, Denmark*

<sup>‡</sup>*Department of Theoretical Chemistry, Lund University, Chemical Centre, P. O. Box 124,  
SE-221 00 Lund, Sweden*

E-mail: mortennp@sdu.dk

## Abstract

We present a systematic investigation of the key components needed to model single chromophore electronic circular dichroism (ECD) within the polarizable embedding (PE) approach. By relying on accurate forms of the embedding potential, where especially the inclusion of local field effects are in focus, we show that qualitative agreement between rotatory strength parameters calculated by full quantum mechanical calculations and the more efficient embedding calculations can be obtained. An important aspect in the computation of reliable absorption parameters is the need for conformational sampling. We show that a significant number of snapshots are needed to avoid artifacts in the calculated electronic circular dichroism parameters due to insufficient configurational sampling thus highlighting the efficiency of the PE model.

# 1 Introduction

Electronic circular dichroism (ECD) is a key spectroscopic technique used to characterize molecules. For example, it can be used in the process of determining the absolute configuration of chiral molecules. For this, modeling of ECD parameters has been a great subject of interest, and particular attention has been paid to the use of quantum mechanical (QM) methods since these have proven to yield both accurate and predictive results.<sup>1-4</sup> Experimental ECD spectra are typically recorded for condensed-phase samples. It can therefore be important to include the effects of the chromophore’s environment, e.g. a solvent, in the quantum chemical calculations. In principle, a straightforward approach is to use a supermolecular cluster scheme where the chromophore and a number of molecules in the environment are all described quantum mechanically. However, this approach can be problematic. First of all, in such calculations there are molecules exposed to a vacuum which can lead to artificial edge effects.<sup>5-7</sup> Further, environment effects on spectroscopic properties may potentially be very long-ranged and indeed a substantial number of molecules must be included to obtain converged results.<sup>5,8-10</sup> Considering recent advances in method formulations and algorithms<sup>11</sup> - as well as the continued development of more efficient computational platforms - density functional theory (DFT) has become the method of choice when considering large molecular clusters. In addition, its time-dependent formulation (TDDFT) may be used to address general response properties including electronic excitation energies and transition strengths relevant for construction of e.g. UV absorption spectra.<sup>12</sup> However, some approximate exchange-correlation functionals may introduce artificial charge-transfer states that are very low in energy, and may therefore lead to artifacts in the predicted results.<sup>5</sup> Furthermore, the issue of conformational sampling means that one generally needs to perform not only one but a number of similar calculations, thus increasing the computational cost drastically. Methods that are more efficient than supermolecular calculations are therefore generally preferred.

In contrast to a full QM treatment of the system, another strategy is to restrict the num-

ber of atoms treated quantum mechanically and describe the remaining atoms in a classical fashion. By this, one way to represent the environment is to use molecular mechanics (MM) leading to the so-called hybrid QM/MM approach.<sup>13</sup> A key concern when using QM/MM-like approaches is the quality of the embedding potential, i.e. the quality of the MM parameters used to represent the electrostatic potential and maybe also non-electrostatic terms. Typical calculations that utilize a QM/MM approach are based on an embedding potential that is constructed on the basis of fixed point charges which are located at the position of the atoms that define the molecular environment. However, including higher-order atom-centered multipoles and atom-centered polarizabilities in the embedding potential greatly increases the accuracy of the embedding potential as opposed to non-polarizable embedding potentials.<sup>14</sup> Such a division of a composite system into two regions treated at different levels of theory greatly reduces the computational cost compared to the cluster approach thus defining a potential route for efficient inclusion of structural dynamical effects into the response property calculations.

Recently, with the increasing computational power and development of more efficient algorithms, it has become possible to study the convergence of response properties with respect to the size of the quantum region.<sup>5</sup> Such studies have typically been performed in connection with a QM/MM approach to capture long-range effects but using a non-polarizable embedding potential. The general conclusion from such studies is that very large quantum regions are needed in order to reach convergence of the calculated properties.<sup>5,10,15</sup> However, by relying on more accurate forms of the embedding potential, smaller quantum regions are typically needed, thereby reducing the computational cost of the calculations.<sup>16,17</sup> In addition, the inclusion of local field effects in the embedding formalism can be crucial when the aim is to reproduce the results obtained from a full QM cluster calculation. Such local field effects have previously been introduced in polarizable continuum models (PCMs)<sup>18</sup> where they are known as cavity field (CF) effects.<sup>19–29</sup> Although QM/MM approaches have been used to study ECD parameters,<sup>30–34</sup> we here introduce the QM/MM equivalent of the

CF effect known as the effective external field (EEF) effect.<sup>35</sup> From a computational point of view ECD spectroscopy is assessed by the calculation of rotatory strengths,<sup>36–41</sup> and in this paper we employ the polarizable embedding (PE) approach<sup>42,43</sup> to model the effects of the environment, here a solvent, on the rotatory strengths including also the above discussed EEF effect.

## 2 Methodology

Our computational strategy is based on the PE model,<sup>42,43</sup> which has been implemented for different wave function approaches,<sup>42,44–48</sup> but here we rely on the implementation within DFT (PE-DFT).<sup>42</sup> The PE model has been formulated within standard response theory<sup>42,43</sup> as well as damped response theory.<sup>49</sup> In this work we use the standard response theory formulation, but the conclusions drawn are equally valid within the damped response formalism.

The PE model is a variant of the QM/MM approach, thus dividing the total system into a quantum part - treated using a QM method - and a classical part - described by *ab-initio*-derived atom-centered multipole moments and dipole–dipole polarizabilities. The interactions between the quantum- and classical regions are described through an embedding operator,  $\hat{v}^{\text{emb}}$ , which is added to the conventional vacuum Kohn-Sham (KS) operator,  $\hat{f}^{\text{KS}}$ , thus forming an effective KS operator

$$\hat{f}^{\text{eff}} = \hat{f}^{\text{KS}} + \hat{v}^{\text{emb}} . \quad (1)$$

The embedding operator is further divided into a part that describes the permanent charge distribution of the environment,  $\hat{v}^{\text{es}}$ , and the induction (polarization) operator,  $\hat{v}^{\text{ind}}$ , that describes the induced charge distribution of the environment

$$\hat{v}^{\text{emb}} = \hat{v}^{\text{es}} + \hat{v}^{\text{ind}} . \quad (2)$$

Note that the operator  $\hat{v}^{\text{ind}}$  depends explicitly on the electron density, meaning that the polarization is calculated based on a double self-consistent-field procedure. For further details regarding the construction of  $\hat{v}^{\text{es}}$  and  $\hat{v}^{\text{ind}}$  see references 42 and 43.

A convenient way of addressing excited states and their properties is through response theory.<sup>50,51</sup> In the case of an isotropic molecular medium, the ECD response, originating from a transition from the ground state  $|0\rangle$  to an excited state  $|n\rangle$ , relates to the residue of the mixed electric-dipole-magnetic-dipole polarizability tensor. Thus the ECD rotatory strength - given in length gauge - is

$$R_{n0} = \text{Im}(\langle 0 | \hat{\boldsymbol{\mu}} | n \rangle \cdot \langle n | \hat{\mathbf{m}} | 0 \rangle) \quad (3)$$

where  $\hat{\boldsymbol{\mu}}$  is the electric dipole operator and  $\hat{\mathbf{m}}$  is the magnetic dipole operator. In practical calculations such a residue is calculated on the basis of the solutions to a generalized eigenvalue problem involving the electronic Hessian and a generalized overlap matrix.<sup>50</sup> The additional contributions to the Hessian stemming from the polarizable environment can be described as two separate contributions:<sup>42</sup> a zeroth-order contribution, which corresponds to modified orbital energies, and a contribution that describes the dynamical response of the environment due to the localized electronic excitation. In addition, as discussed in detail below, the property gradient is also modified due to the applied perturbation.<sup>35</sup>

To avoid origin-dependent results of the rotatory strength, due the origin-dependence of the magnetic dipole operator, gauge-including atomic orbitals (GIAOs) can be used.<sup>16,52-55</sup> Finally, the predicted rotatory strengths are used in combination with either Lorentzian or Gaussian band profiles to simulate the ECD spectrum<sup>56</sup> with the latter being used in this work.

Local field effects, which among other are important in the study of molecular absorption intensities, depend on the polarization of the environment induced by the externally applied perturbation. The PE model discussed above was originally formulated without taking

this into account. However, recently the direct coupling between the external electric field and the environment was developed and implemented, resulting in an extension of the PE model.<sup>35</sup> Calculations that include EEF effects are denoted PE(EEF) in this work while those without EEF effects are denoted PE. The ECD rotatory strength in the PE(EEF) formalism can easily be obtained by substituting the electric transition moment of eq 3 by the effective electric transition dipole moment,  $\bar{\boldsymbol{\mu}}$ , obtained as

$$\bar{\boldsymbol{\mu}} = \boldsymbol{\mu} + \tilde{\boldsymbol{\mu}} \quad (4)$$

where  $\boldsymbol{\mu}$  is the normal electric dipole transition moment and  $\tilde{\boldsymbol{\mu}}$  is the contribution to the electric dipole transition moment due to the direct coupling between the environment and the externally applied electric field. The quantity  $\tilde{\boldsymbol{\mu}}$ , in the PE(EEF) formalism, is obtained by

$$\tilde{\boldsymbol{\mu}}^{\text{PE(EEF)}} = - \sum_{s=1}^S \hat{\mathbf{F}}_s^e \frac{\partial [\boldsymbol{\mu}_s^{\text{ind}}]^T}{\partial \mathbf{F}^{\omega, \text{ext}}} . \quad (5)$$

Here we have introduced a sum over all sites,  $S$ , in the environment that contain a polarizability which in turn induces a local dipole moment,  $\boldsymbol{\mu}_s^{\text{ind}}$ . Furthermore,  $\hat{\mathbf{F}}_s^e$  is the electric field operator involving site  $s$  and  $\mathbf{F}^{\omega, \text{ext}}$  is the external electric field.

A practical aspect of the PE model, and QM/MM schemes in general, is the need to explicitly include conformational sampling, in contrast to models that employ a continuum description of the solvent where conformational sampling is implicitly included. This is usually obtained by considering a number of snapshots extracted from a molecular dynamics (MD) trajectory. The environment in a continuum description is represented as a dielectric where the solute is enclosed in a cavity, which is typically formed by the union of spheres centered at the individual solute atoms with radii defined by the Van der Waals (vdW) radius of the associated atom. In this way the cavity reflects the molecular shape of the solute. The cavity surface is typically represented by a number of tessera each assigned an area and a charge in the center position. In this paper we use the FixSol method by Thellamurege and

Li<sup>57</sup> which was recently combined with the PE model.<sup>58</sup> The FixSol method is an extension to the family of conductor-like screening models (COSMO)<sup>59–63</sup> where the medium is considered as a conductor with the dielectric constant  $\epsilon = \infty$  with a subsequent scaling of the induced charge distribution to recover the effect of having a finite  $\epsilon$ . The equivalent effect to the local fields, discussed in connection with the PE model, when the molecule is introduced in a dielectric medium is known as the cavity field effect. The quantity  $\tilde{\boldsymbol{\mu}}$  from Eq. 4 is then obtained from

$$\tilde{\boldsymbol{\mu}}^{\text{FixSol}} = - \sum_{k=1}^K \hat{V}_k^e \frac{\partial [q_k^{\text{ind}}]}{\partial \mathbf{F}_n^{\omega, \text{ext}}} \quad (6)$$

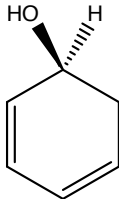
where we have introduced a sum over all tesserae,  $K$ , and  $\hat{V}_k^e$  is the electric potential operator involving site  $k$ . Furthermore,  $\mathbf{F}_n^{\omega, \text{ext}}$  holds the normal components of the externally applied field. The induced charges are determined by

$$q_k^{\text{ind}} = - \frac{\epsilon}{\epsilon - 1} \sum_l D_{kl}^{-1} (\mathbf{F}^{\omega, \text{ext}} \cdot \hat{\mathbf{n}})_l \quad (7)$$

where  $\hat{\mathbf{n}}$  is the outward pointing vector perpendicular to each tessera, and  $\mathbf{D}$  is the matrix describing the solvent polarization due to a perturbing electric field.<sup>64</sup>

### 3 Computational details

All calculations of rotatory strengths were carried out using a development version of the Dalton program<sup>65</sup> interfaced with the PE library<sup>66</sup> and Gen1Int.<sup>67,68</sup> In order to obtain

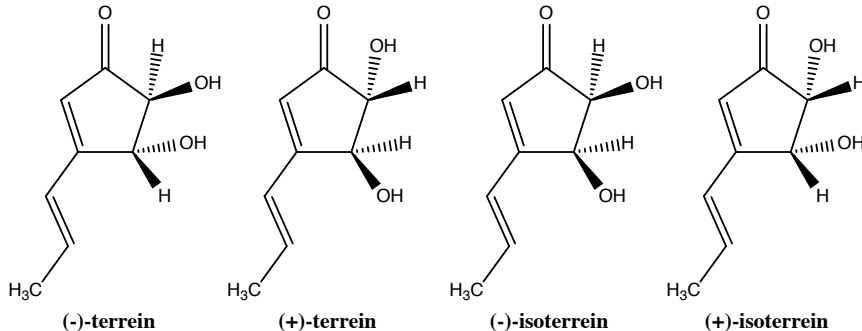


Scheme 1: (S)-cyclohex-2,4-dienol.

gauge-invariant results we used the implementation of Ruud and Helgaker<sup>69</sup> which applies



standard time-independent GIAOs. For the purpose of analyzing the components needed to compute the rotatory strength we consider the (S)-cyclohex-2,4-dienol molecule (illustrated in Scheme 1) solvated in water. Furthermore, to illustrate the importance of conformational



Scheme 2: The four stereoisomers of terrein.

sampling we consider the set of four stereoisomers of terrein (illustrated in Scheme 2) solvated in acetonitrile.

The embedding potential representing the solvent molecules consists of distributed multipole moments up to second order (quadrupoles) and distributed dipole-dipole polarizabilities unless otherwise noted. The expansion centers for the distributed multipoles and polarizabilities were placed at the atomic nuclei that define the environment. All distributed multipoles and polarizabilities were derived by utilizing the LoProp approach<sup>70</sup> employing the LoProp for Dalton script<sup>71</sup> based on integrals and response functions obtained from the Dalton program package.<sup>65</sup>

For the analysis of the rotatory strength of (S)-cyclohex-2,4-dienol we consider a single conformation extracted from the last frame of a one nanosecond molecular dynamics trajectory produced using the Desmond MD package<sup>72–74</sup> as distributed by Schrödinger.<sup>75</sup> The MD simulation workflow was run with the default parameters in the Maestro interface to Desmond. The OPLS 2005 force field<sup>72</sup> was chosen to represent (S)-cyclohex-2,4-dienol, while water molecules were added in a cubic box to a distance of 20 Å in all principle directions measured from the solute, yielding a total of 3083 water molecules all represented using the TIP3P<sup>76,77</sup> water model. For the subsequent PE-QM calculations, spherical cuts

around (S)-cyclohex-2,4-dienol were extracted from this frame including all water molecules within the radius of the sphere.

All PE-QM calculations of (S)-cyclohex-2,4-dienol solvated in water utilized the CAM-B3LYP functional<sup>78</sup> and the 6-31+G\* basis set<sup>79–82</sup> to represent the solute while the 6-31G\* basis set was used for water molecules included in the quantum region. Multipoles and polarizabilities of the water molecules in the classical region were calculated at the same level of theory as the quantum mechanically treated water molecules, i.e. CAM-B3LYP/6-31G\*. When including FixSol in the calculations, atomic radii of 1.40, 2.10 and 1.90 Å were used for the H, C, and O atoms, respectively, to define the molecular cavity. For the ground-state wave-function optimization we used a static dielectric constant of  $\epsilon = 78.39$  whereas for the transition property calculations we used  $\epsilon_{\text{inf}} = 1.776$ .

The QM/MM MD simulations that were used to generate geometries of the four stereoisomers of terrein in acetonitrile were carried out in the *sander* module in AMBER.<sup>83</sup> The simulations utilized the PM6-DH+<sup>84</sup> method for terrein while the acetonitrile molecules were described using a classical six-site model.<sup>85</sup> Each of the four stereoisomers of terrein and the acetonitrile molecules were initially minimized with the conjugate gradient minimizer for 1000 steps before an initial equilibration for 50 ps in the NVT ensemble at 300 K followed by an additional equilibration for 50 ps in the NPT ensemble at 300 K and a pressure of 1 bar. To obtain adequate sampling, each of the four stereoisomers was first run for 1 ns in the NPT ensemble. One hundred snapshots were subsequently extracted from each of the 1 ns trajectories and used as starting points for additional 2 ns simulations for a total of 0.8  $\mu\text{s}$  simulation time. Snapshots were extracted from each trajectory at 0.5 ns, 1.0 ns, 1.25 ns, 1.5 ns, 1.75 ns and 2.0 ns for a total of 600 snapshots per stereoisomer (2400 in total). Excitation energies, oscillator strengths, and rotatory strengths were computed at the PE-B3LYP<sup>86–88</sup>/pcseg-2<sup>89</sup> level of theory for each snapshot. Acetonitrile parameters were computed with the B3LYP functional and an ANO-type recontraction of the aug-cc-pVDZ<sup>90</sup> basis set as required by the LoProp procedure. See supporting information for additional

computational details.

## 4 Results and discussion

In this section we consider initially two approaches aimed at modeling solvent effects on the rotatory strength of (S)-cyclohex-2,4-dienol. We first consider a cluster approach in which all solvent molecules are treated at the quantum mechanical level. By characterizing the orbitals involved in the transition under study we can rule out that we are dealing with an intruding charge-transfer state as observed for similar cluster calculations,<sup>5-7,91,92</sup> meaning that this approach will allow us to establish a proper reference for further approximate calculations. Next we consider the PE-QM approach with or without EEF effects. The solute is always treated using quantum mechanics while the solvent effects are incorporated through an embedding potential, either as a classical potential made from permanent multipoles and polarizabilities, or through a dielectric continuum description. Another aspect which can be important to consider when calculating ECD parameters is the finite-temperature effects. We address this issue by collecting snapshots of four stereoisomers of terrein embedded in acetonitrile solution from MD trajectories and compute the ECD spectrum for each snapshot.

### 4.1 Cluster approach

It has previously been reported that DFT based electronic structure calculations using approximate functionals on large cluster systems may suffer from spurious low-lying charge-transfer states originating from the solvent molecules positioned at the edge of the cluster.<sup>5-7,91,92</sup> This will typically be the case when the solvent molecules are exposed to a vacuum.<sup>93</sup> When considering a response theory approach, where the excited states are found by locating residues of the appropriate response function, this is particularly problematic as one need to resolve an increasing number of states in order to determine the relevant state(s). Hence it is important to analyze the calculated states in order not to compare

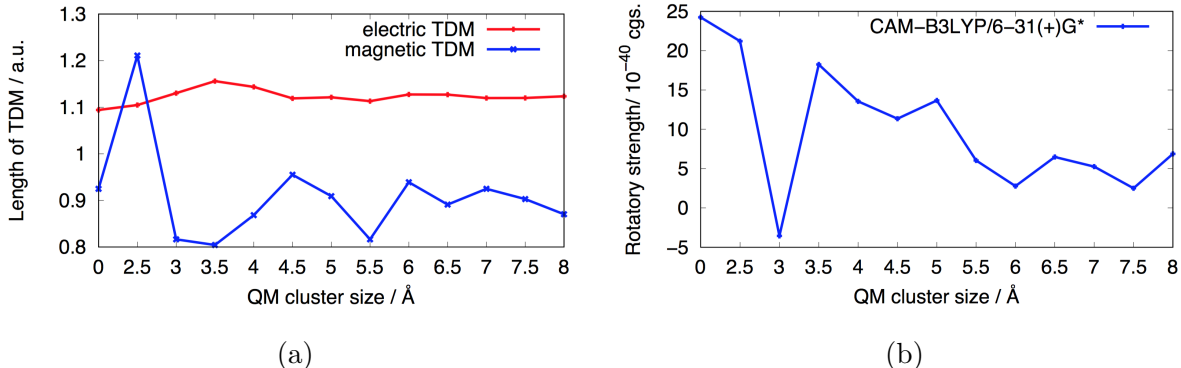


Figure 1: (a) Convergence of the electric- and magnetic transition dipole moments as a function the sphere radius defining the water molecules included in the full QM calculation. (b) Rotatory strength parameters based on full QM calculations. Zero QM cluster size indicates that only the solute has been included in the calculation.

states containing spurious charge-transfer from edge solvent molecules. In our case, however, the bright  $\pi \rightarrow \pi^*$  transition remains lowest at any finite cluster size considered. For the largest cluster we consider (including all solvent molecules within a distance of 8 Å from the solute corresponding to 148 water molecules) the  $\pi \rightarrow \pi^*$  transition is located at 4.715 eV. Based on calculations of the smaller clusters we find that the lowest excitation energy is converged to within 0.015 eV of the 8 Å cluster by including 23 water molecules (3.5 Å cluster; see Figure S4 in the supporting information).

We now move on to analyze the ECD of our solute. As the ECD intensity is related to the rotatory strength given in Eq. 3 we will begin this section focusing on this quantity and its specific elements i.e. the electric- and magnetic transition dipole moments (eTDM/mTDM). In Figure 1a we have illustrated the dependence of the lengths of the eTDM and mTDM, associated with the lowest  $\pi \rightarrow \pi^*$  transition with respect to cluster size treating all molecules quantum mechanically. Comparing the convergence pattern of the two transition dipole moments it is observed that especially the mTDM has a very slow convergence with respect to cluster size as opposed the electric transition moment. Focusing on the eTDM we see that even for very small cluster sizes this quantity is only slightly affected by an increase in the solvent radius. On the other hand the mTDM fluctuates around a value of 0.9 a.u. for all

cluster calculations. Such fluctuations have a large impact on the rotatory strength, which may even change sign as observed for the 3.0 Å cluster (see Figure 1b). Indeed the results obtained using the cluster approach indicates that very large clusters are needed for the rotatory strength to converge with respect to cluster size. Hence for all practical purposes this approach is not applicable, or becomes computationally very expensive at best, when the solute/solvent dynamics are taken into account (as will be discussed in Sec. 4.3).

## 4.2 Polarizable embedding approach

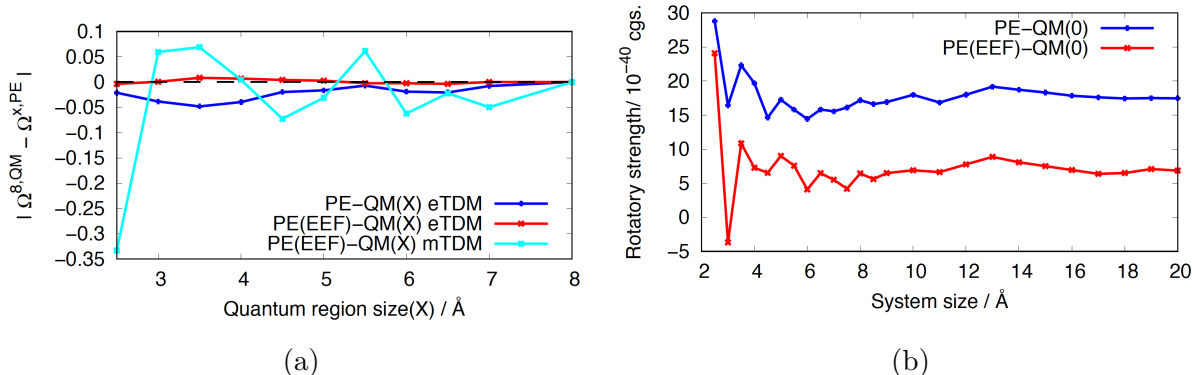


Figure 2: (a) The difference between the electric transition dipole moment calculated using an 8 Å cluster approach and PE-QM, with or without EEF, with varying number of water molecules included in the quantum region. (b) The rotatory strength calculated using PE-QM with or without EEF effects - keeping only the solute in the quantum region - as a function of increasing size of system size.

To test the performance of the PE model, we first use the full QM calculation on the largest cluster as our reference calculation and step-wise convert water molecules from the quantum region to the classical region, thus keeping the system size at 8 Å in all calculations. In the PE-QM calculations we capture the mutual polarization between the quantum region and the remaining solvent molecules in the classical region, and thus we expect the transition moments to converge much faster towards the reference compared to the cluster approach described in the previous section. Note that the analysis presented in Sec. 4.1 was made on the basis of clusters gradually increasing in size, whereas the analysis made in this section

keeps a fixed system size but now differentiates between water molecules being described either classically or based on quantum mechanics.

In Figure 2a we compare the use of the PE model with or without EEF effects by focusing on the deviation in TDMs from the reference calculation for the lowest  $\pi \rightarrow \pi^*$  transition. Focussing on the eTDM, which is the only TDM affected by adding EEF effects, it is evident that the PE(EEF) model yields values that compare much better to the full QM reference than the results obtained without EEF effects included. Indeed, most encouraging, we observe that even the smallest quantum region at 2.5 Å (PE(EEF)-QM(2.5)) - keeping the remaining 5.5 Å water of the initial 8 Å cluster in the classical region - is capable of reproducing the full QM reference satisfactorily. This shows that properties derived only from eTDMs, such as oscillator strengths, benefit substantially from including EEF effects because very small quantum regions can be used. On the other hand, the mTDM is not modified by EEF effects and even for large quantum regions we still observe deviations from the reference compared to that observed for the eTDM. Thus the deviations one can expect in the rotatory strength parameter comparing full QM calculations and PE-QM calculations is dominated by the error made in the mTDM whether EEF is included or not.

Next we address the convergence of the rotatory strength with respect to system size. Figure 2b shows the convergence of the rotatory strength obtained with PE(EEF)-QM(0) with respect to system size, i.e. keeping only the solute in the quantum region and systematically increasing the classical region up to 20 Å. The convergence pattern of the two models are very similar and is reached at approximately a system size of 8 Å, however, not including EEF leads to a much higher rotatory strength for all cluster sizes. Indeed the calculated rotatory strength obtained using PE(EEF)-QM(0) is  $6.86 \cdot 10^{-40}$  cgs, close to the value predicted by the cluster approach in the previous section, and approximately three times lower than the predicted value obtained using PE-QM(0) ( $17.47 \cdot 10^{-40}$  cgs).

Figure 3 shows the difference in rotatory strength for a system size of 20 Å as a function of the quantum-region size using PE(EEF)-QM(7) as reference. As opposed to Figure 2

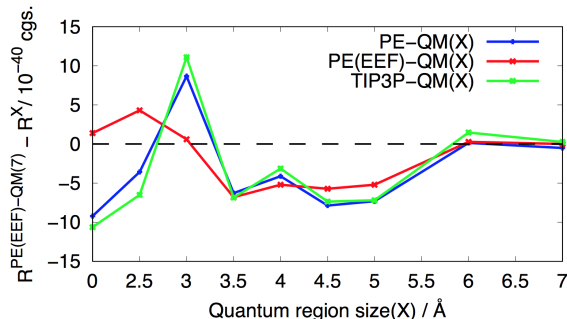


Figure 3: Rotatory strength difference calculated using PE-QM with or without EEF effects as a function of increasing quantum region size (zero indicating that only the solute is included in the quantum region) using PE(EFF)-QM(7) as reference ( $8.25 \cdot 10^{-40}$  cgs). The system is in all cases a 20 Å spherical cluster.

where the focus was to investigate the quantum effects by directly comparing embedding calculations with quantum mechanical calculations we here focus on the convergence of the quantum-region size for a fully converged system size. We thus utilize the largest affordable model as a reference (PE(EFF)-QM(7)). We expect the two models (PE & PE(EFF)) to yield similar results for larger quantum regions and indeed increasing the quantum-region size by more than 3.5 Å yields almost identical results. For the smaller quantum regions we generally observe less deviations from the reference of the rotatory strength when EEF is included which can be attributed to the more accurate eTDMs. Thus, we find that including EEF yields improved rotatory strengths for small quantum regions but it is necessary to include solvent molecules in the quantum region if high accuracy is needed. Furthermore, as seen from Figure 3, representing the water molecules by the TIP3P standard water potential leads to an almost identical behavior of the rotatory strength when expanding the size of the quantum region compared to the use of PE without EEF effects underlining the importance of these effects.

So far the analysis for the ECD parameters have been performed for a single cluster of molecules. However, as will be detailed in the following section, configurational sampling is of utmost importance when the aim is to compare the calculated results to e.g. experimental values. Sampling may be included either explicitly (as discussed in the following section)

or implicitly through use of a dielectric continuum description of the solvent. Based on the FixSol continuum model - and including only the solute in the cavity - we obtain for (S)-cyclohex-2,4-dienol a rotatory strength of  $33.37 \cdot 10^{-40}$  cgs when including the effects of the cavity field. Such results cannot directly be compared to their PE counterparts without introducing configurational averaging - a point which will be elaborated in the following section.

### 4.3 The four stereoisomers of terrein

To demonstrate the implementation and computational protocol presented above we present in this section UV/Vis absorption and ECD spectra of the four stereoisomers of terrein (depicted in Scheme 2) in acetonitrile solvent. The two stereocenters in terrein allow for a total of four unique stereoisomers:  $(\pm)$ -terrein and  $(\pm)$ -isoterrein. The hydroxyl groups attached to the cyclopentenone ring in terrein are in *trans* configuration whereas they are in *cis* configuration in isoterrein. Figure 4 shows the UV/Vis absorption and ECD spectra

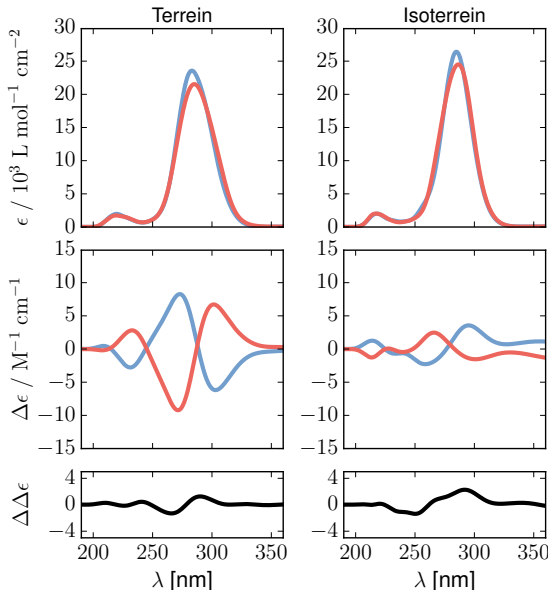


Figure 4: Computed absorption spectrum and electronic circular dichroism spectrum in the top and middle row, respectively, for  $(\pm)$ -terrein and  $(\pm)$ -isoterrein in the left and right column, respectively [(+) is red and (-) is blue]. The bottom row shows the sum of the ECD spectra for two stereoisomers.



of the four stereoisomers of terrein. In these calculations 600 snapshots have been used to construct each of the spectra as detailed in the Computational details section.

The UV/Vis absorption spectra for terrein and isoterrein (top row in Figure 4) are, as expected, very similar. All four stereoisomers of terrein show a major absorption peak around 285 nm due to a strong  $\pi \rightarrow \pi^*$  transition with an additional minor absorption peak at 215 nm. The computed UV/Vis spectra for either terrein or isoterrein for both the (+) and (−) configurations are overlapping which indicates convergence with respect to the number of snapshots included. To quantify how a spectrum  $S$  converges towards a reference spectrum we use the integral:<sup>94,95</sup>

$$\delta_{\text{dev}}(S, N) = \frac{\int_{\omega_{\min}}^{\omega_{\max}} |S_N(\omega) - S_{600}(\omega)| d\omega}{\int_{\omega_{\min}}^{\omega_{\max}} |S_{600}(\omega)| d\omega} \quad (8)$$

where  $S_N(\omega)$  is the spectrum obtained by including only  $N$  snapshots in the averaging and  $S_{600}$  is the reference spectrum obtained by using all 600 snapshots for each stereoisomer. The integral limits  $\omega_{\min}$  and  $\omega_{\max}$  are defined in this work by the frequency range of the spectrum in Figure 4. For UV/Vis absorption this deviation is plotted in the top row in Figure 5 for (±)-terrein and (±)-isoterrein, respectively. The percentage-wise deviation is initially around 35 % when only 10 snapshots are included but quickly reaches a 10 % deviation when 100 snapshots are included or below 5 % when 300 snapshots are included (see Figures S3 and S4 in the supporting information for the spectra.) Such a low deviation in the computed UV/Vis absorption spectra is not unexpected since convergence has previously been shown to be obtainable with around 100 snapshots for solute-solvent systems.<sup>96</sup> However, computed ECD spectra are more sensitive to structural and environmental effects and generally require a larger number of snapshots to be included.<sup>95</sup> ECD spectra are shown for the stereoisomers for terrein and isoterrein, respectively, in the middle row in Figure 4. Both spectra show the expected opposite sign between the stereoisomers. The ECD spectrum for (±)-terrein shows major peaks at 230, 270 and 305 nm. For (±)-isoterrein the three peaks in the

ECD spectrum are located at slightly shorter wavelengths, namely around 210, 260 and 290 nm and with noticeably smaller intensities than what was observed for ( $\pm$ )-terrein. In general, the features of all four ECD curves are similar in the sense that there is a sign change between all major peaks. For example, the Cotton effect for the three major peaks of (+)-terrein is positive, negative and finally positive. Using Eq. 8 to quantify how the

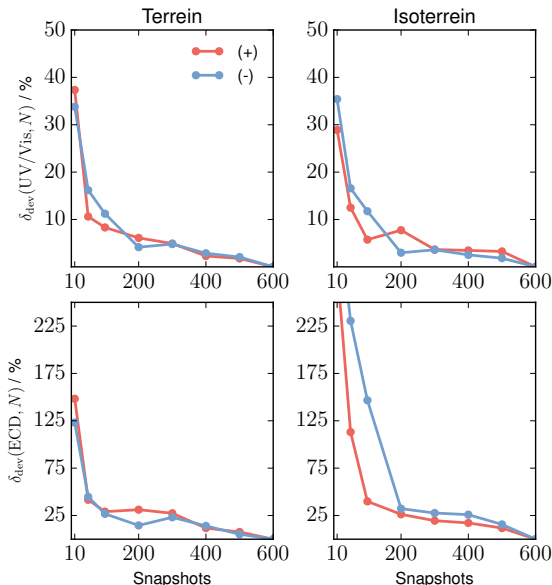


Figure 5: Percentage error of computed UV/Vis (top row) and ECD (bottom row) spectra as a function of snapshots included in the averaging compared to the spectrum obtained by including all 600 snapshots for each stereoisomer of terrein and isoterrein.

individually computed ECD spectra converge as the number of snapshots is increased we observe (Figure 5 bottom row) that the deviation is much larger for ECD than it was for UV/Vis absorption. Initial deviations for terrein and isoterrein are larger than 125 % and 250 %, respectively. The convergence is observed to follow that of the UV/Vis spectra but with larger deviations. Even when including 200 snapshots the deviation is still around 25 % and converges only slowly towards the reference value. As has been touched upon above, this is due to the solvent molecules causing large changes in the rotatory strength between different snapshots.

A final measure on how well the ECD spectrum is converged is presented in the bottom row of Figure 4 where we have computed the difference ECD spectrum, that is, the two

ECD spectra in a column added together. In an ideal situation with perfect sampling of the stereoisomers of terrein, the ECD spectra of two stereoisomers should match exactly with a sign difference and the difference ECD spectrum should be zero for all wavelengths. In practice, the difference ECD spectrum will deviate from zero as a result of the insufficient configurational sampling discussed above. Here, Eq. 8 is not suitable as a metric because the integral in the denominator would go towards zero faster than the difference in the numerator. Instead we compute the mean, mean absolute error (MAE) and root mean square error (RMSE) of the difference ECD spectra as presented in Table 1. We observe

Table 1: Mean, mean absolute error (MAE) and root mean square error (RMSE) of difference ECD plots as a function of included snapshots in the averaging. Units are  $\text{M}^{-1} \text{cm}^{-1}$ .

|            |      | Number of Snapshots |     |     |     |     |     |
|------------|------|---------------------|-----|-----|-----|-----|-----|
|            |      | 100                 | 200 | 300 | 400 | 500 | 600 |
| terrein    | mean | -0.3                | 0.3 | 0.3 | 0.1 | 0.1 | 0.0 |
|            | MAE  | 0.7                 | 1.0 | 0.5 | 0.3 | 0.5 | 0.3 |
|            | RMSE | 0.9                 | 1.3 | 0.6 | 0.5 | 0.7 | 0.5 |
| isoterrein | mean | 0.8                 | 0.0 | 0.1 | 0.2 | 0.1 | 0.3 |
|            | MAE  | 1.7                 | 0.8 | 0.6 | 0.7 | 0.6 | 0.7 |
|            | RMSE | 2.2                 | 1.1 | 0.8 | 1.0 | 0.8 | 0.9 |

that the mean of the difference ECD spectra converges quickly to values oscillating close to zero from around 200 snapshots for both terrein and isoterrein. Care should be taken though, not to put too much significance to the mean of the difference ECD spectra when there is no other data to back up the conclusions. We demonstrated in Figure 5 that the convergence was rather slow for the absolute spectra and thus conclude that although the mean looks favorable, it is a mere fortuitous cancellation due to sign changes in the difference ECD spectra. Therefore, we instead use the MAE and RMSE of the difference ECD spectra as a more robust metric to quantify convergence. As the number of snapshots is increased we observe that the MAEs (RMSEs) converge from around 300 snapshots after which they are in the  $0.3 - 0.5 \text{ M}^{-1} \text{cm}^{-1}$  ( $0.5 - 0.7 \text{ M}^{-1} \text{cm}^{-1}$ ) range in the case of terrein and  $0.6 - 0.7 \text{ M}^{-1} \text{cm}^{-1}$  ( $0.8 - 1.0 \text{ M}^{-1} \text{cm}^{-1}$ ) in the case of isoterrein.

In summary, we have investigated multiple metrics in order to quantify convergence of

solute-solvent UV/Vis and ECD spectra. We note in particular that the number of snapshots to include when computing ECD spectra are much larger than the corresponding UV/Vis spectra.

## 5 Conclusion

In this paper we have investigated several approaches for the calculation of rotatory strengths of solvated molecules. In order to establish a proper reference, from which less accurate but efficient models can be benchmarked against, we have first of all calculated the rotatory strength based on a supermolecular cluster approach. Our results show that this approach requires that a substantial number of solvent molecules need to be included in the quantum mechanical calculation in order to reach convergence of the rotatory strength. As an alternative to the cluster approach we benchmarked the polarizable embedding (PE) model with or without local-field corrections, i.e. the so-called effective external field (EEF) effect, against the cluster approach. Our results show that by using the PE model we are able to qualitatively reproduce the rotatory strength calculated using the supermolecular cluster approach. Furthermore, we find that the inclusion of EEF effects yields better convergence with respect to quantum-region size. However, if highly accurate rotatory strengths are needed it is necessary to include some solvent molecules in the quantum region because of the sensitivity of the magnetic transition moment. We further show, for the case of the four stereoisomers of terrein, that the rotatory strength is heavily dependent on the number of snapshots considered which highlights the need for a computationally feasible and reliable methodology.

## Acknowledgement

Computational resources were provided by the DeIC National HPC Center at the University of Southern Denmark through an Abacus 2.0 grant. J. M. H. O. acknowledges financial support from the Carlsberg Foundation (grant id. CF15-0823). C. S. thanks the Danish Council for Independent Research (the Sapere Aude program) for financial support (Grant no. DFF 4181-00370). J. K. thanks the Danish Council for Independent Research (the Sapere Aude program) and the Villum Foundation for financial support.

## References

- (1) Crawford, T. D. Ab initio calculation of molecular chiroptical properties. *Theo. Chem. Acc.* **2005**, *115*, 227–245.
- (2) Autschbach, J. In *Comprehensive Chiroptical Spectroscopy*; Berova, N., Polavarapu, P. L., Nakanishi, K., Woody, R. W., Eds.; Wiley, 2012; Vol. 1; pp 593–642.
- (3) Crawford, T. D. In *Comprehensive Chiroptical Spectroscopy*; Berova, N., Polavarapu, P. L., Nakanishi, K., Woody, R. W., Eds.; Wiley, 2012; Vol. 1; pp 675–697.
- (4) Goerigk, L.; Kruse, H.; Grimme, S. In *Comprehensive Chiroptical Spectroscopy*; Berova, N., Polavarapu, P. L., Nakanishi, K., Woody, R. W., Eds.; Wiley, 2012; Vol. 1; pp 643–674.
- (5) Isborn, C. M.; Mar, B. D.; Curchod, B. F. E.; Tavernelli, I.; Martínez, T. J. The Charge Transfer Problem in Density Functional Theory Calculations of Aqueously Solvated Molecules. *J. Phys. Chem. B* **2013**, *117*, 12189–12201.
- (6) Lange, A.; Herbert, J. M. Simple Methods To Reduce Charge-Transfer Contamination

- in Time-Dependent Density-Functional Calculations of Clusters and Liquids. *J. Chem. Theory Comput.* **2007**, *3*, 1680–1690.
- (7) Neugebauer, J.; Louwerse, M. J.; Baerends, E. J.; Wesolowski, T. A. The merits of the frozen-density embedding scheme to model solvatochromic shifts. *J. Chem. Phys.* **2005**, *122*, 094115.
  - (8) Kulik, H. J.; Zhang, J.; Klinman, J. P.; Martínez, T. J. How Large Should the QM Region Be in QM/MM Calculations? The Case of Catechol O-Methyltransferase. *J. Phys. Chem. B* **2016**, *120*, 11381–11394.
  - (9) Provorse, M. R.; Peev, T.; Xiong, C.; Isborn, C. M. Convergence of Excitation Energies in Mixed Quantum and Classical Solvent: Comparison of Continuum and Point Charge Models. *J. Phys. Chem. B* **2016**, *120*, 12148–12159.
  - (10) Milanese, J. M.; Provorse, M. R.; Alameda, E.; Isborn, C. M. Convergence of Computed Aqueous Absorption Spectra with Explicit Quantum Mechanical Solvent. *J. Chem. Theory Comput.* **2017**, *13*, 2159–2171.
  - (11) Bowler, D. R.; Miyazaki, T.  $\mathcal{O}(N)$  methods in electronic structure calculations. *Reports on Progress in Physics* **2012**, *75*, 036503.
  - (12) Dreuw, A.; Head-Gordon, M. Single-Reference ab Initio Methods for the Calculation of Excited States of Large Molecules. *Chem. Rev.* **2005**, *105*, 4009–4037.
  - (13) Warshel, A.; Levitt, M. Theoretical studies of enzymic reactions: Dielectric, electrostatic and steric stabilization of the carbonium ion in the reaction of lysozyme. *J. Mol. Bio.* **1976**, *103*, 227–249.
  - (14) Olsen, J. M. H.; List, N. H.; Kristensen, K.; Kongsted, J. Accuracy of Protein Embedding Potentials: An Analysis in Terms of Electrostatic Potentials. *J. Chem. Theory Comput.* **2015**, *11*, 1832–1842.

- (15) Flaig, D.; Beer, M.; Ochsenfeld, C. Convergence of Electronic Structure with the Size of the QM Region: Example of QM/MM NMR Shieldings. *J. Chem. Theory Comput.* **2012**, *8*, 2260–2271.
- (16) Steinmann, C.; Olsen, J. M. H.; Kongsted, J. Nuclear Magnetic Shielding Constants from Quantum Mechanical/Molecular Mechanical Calculations Using Polarizable Embedding: Role of the Embedding Potential. *J. Chem. Theory Comput.* **2014**, *10*, 981–988.
- (17) Schwabe, T.; Beerepoot, M. T. P.; Olsen, J. M. H.; Kongsted, J. Analysis of computational models for an accurate study of electronic excitations in GFP. *Phys. Chem. Chem. Phys.* **2015**, *17*, 2582–2588.
- (18) Tomasi, J.; Mennucci, B.; Cammi, R. Quantum Mechanical Continuum Solvation Models. *Chem. Rev.* **2005**, *105*, 2999–3094.
- (19) Miertuš, S.; Scrocco, E.; Tomasi, J. Electrostatic interaction of a solute with a continuum. A direct utilization of AB initio molecular potentials for the prevision of solvent effects. *Chem. Phys.* **1981**, *55*, 117–129.
- (20) Cammi, R.; Tomasi, J. Remarks on the use of the apparent surface charges (ASC) methods in solvation problems: Iterative versus matrix-inversion procedures and the renormalization of the apparent charges. *J. Comp. Chem.* **1995**, *16*, 1449–1458.
- (21) Cammi, R.; Cappelli, C.; Corni, S.; Tomasi, J. On the Calculation of Infrared Intensities in Solution within the Polarizable Continuum Model. *J. Phys. Chem. A* **2000**, *104*, 9874–9879.
- (22) Corni, S.; Cappelli, C.; Cammi, R.; Tomasi, J. Theoretical Approach to the Calculation of Vibrational Raman Spectra in Solution within the Polarizable Continuum Model. *J. Phys. Chem. A* **2001**, *105*, 8310–8316.

- (23) Cappelli, C.; Corni, S.; Mennucci, B.; Cammi, R.; Tomasi, J. Vibrational Circular Dichroism within the Polarizable Continuum Model: A Theoretical Evidence of Conformation Effects and Hydrogen Bonding for (S)-(-)-3-Butyn-2-ol in CCl<sub>4</sub>Solution. *J. Phys. Chem. A* **2002**, *106*, 12331–12339.
- (24) Pecul, M.; Lamparska, E.; Cappelli, C.; Frediani, L.; Ruud, K. Solvent Effects on Raman Optical Activity Spectra Calculated Using the Polarizable Continuum Model. *J. Phys. Chem. A* **2006**, *110*, 2807–2815.
- (25) Cappelli, C.; Rizzo, A.; Mennucci, B.; Tomasi, J.; Cammi, R.; Rikken, G. L. J. A.; Mathevet, R.; Rizzo, C. The Cotton–Mouton effect of furan and its homologues in the gas phase, for the pure liquids and in solution. *J. Chem. Phys.* **2003**, *118*, 10712–10724.
- (26) Cappelli, C.; Mennucci, B.; Cammi, R.; Rizzo, A. Quantum Mechanical Polarizable Continuum Model Approach to the Kerr Effect of Pure Liquids. *J. Phys. Chem. B* **2005**, *109*, 18706–18714.
- (27) Cammi, R.; Mennucci, B.; Tomasi, J. An Attempt To Bridge the Gap between Computation and Experiment for Nonlinear Optical Properties: Macroscopic Susceptibilities in Solution†. *J. Phys. Chem. A* **2000**, *104*, 4690–4698.
- (28) Ferrighi, L.; Frediani, L.; Cappelli, C.; Salek, P.; Ågren, H.; Helgaker, T.; Ruud, K. Density-functional-theory study of the electric-field-induced second harmonic generation (EFISHG) of push–pull phenylpolyenes in solution. *Chem. Phys. Lett.* **2006**, *425*, 267–272.
- (29) Pipolo, S.; Cammi, R.; Rizzo, A.; Cappelli, C.; Mennucci, B.; Tomasi, J. Cavity field effects within a polarizable continuum model of solvation: Application to the calculation of electronic circular dichroism spectra of R-(+)-3-methyl-cyclopentanone. *Int. J. Quant. Chem.* **2010**, *111*, 826–838.



- (30) Jensen, L.; Swart, M.; van Duijnen, P. T.; Autschbach, J. Circular dichroism spectrum of  $[\text{Co}(\text{en})_3]^{3+}$  in water: A discrete solvent reaction field study. *Int. J. Quant. Chem.* **2006**, *106*, 2479–2488.
- (31) Egidi, F.; Russo, R.; Carnimeo, I.; D’Urso, A.; Mancini, G.; Cappelli, C. The Electronic Circular Dichroism of Nicotine in Aqueous Solution: A Test Case for Continuum and Mixed Explicit-Continuum Solvation Approaches. *J. Phys. Chem. A* **2015**, *119*, 5396–5404.
- (32) Gattuso, H.; Assfeld, X.; Monari, A. *9th Congress on Electronic Structure: Principles and Applications (ESPA 2014)*; Springer Berlin Heidelberg, 2015; pp 225–232.
- (33) Gattuso, H.; Spinello, A.; Terenzi, A.; Assfeld, X.; Barone, G.; Monari, A. Circular Dichroism of DNA G-Quadruplexes: Combining Modeling and Spectroscopy To Unravel Complex Structures. *J. Phys. Chem. B* **2016**, *120*, 3113–3121.
- (34) Pikulska, A.; Steindal, A. H.; Beerepoot, M. T. P.; Pecul, M. Electronic Circular Dichroism of Fluorescent Proteins: A Computational Study. *J. Phys. Chem. B* **2015**, *119*, 3377–3386.
- (35) List, N. H.; Jensen, H. J. A.; Kongsted, J. Local electric fields and molecular properties in heterogeneous environments through polarizable embedding. *Phys. Chem. Chem. Phys.* **2016**, *18*, 10070–10080.
- (36) Hansen, A. E.; Bouman, T. D. *Advances in Chemical Physics*; John Wiley & Sons, Inc., pp 545–644.
- (37) Bouman, T. D.; Hansen, A. E.; Voigt, B.; Rettrup, S. Large-scale RPA calculations of chiroptical properties of organic molecules: Program RPAC. *Int. J. Quant. Chem.* **1983**, *23*, 595–611.

- (38) Carnell, M.; Peyerimhoff, S.; Breest, A.; Gödderz, K.; Ochmann, P.; Hormes, J. Experimental and quantum-theoretical investigation of the circular dichroism spectrum of R-methyloxirane. *Chem. Phys. Lett.* **1991**, *180*, 477–481.
- (39) Carnell, M.; Grimme, S.; Peyerimhoff, S. Theoretical study of the circular dichroism and VUV spectra of trans-2, 3-dimethyloxirane. *Chem. Phys.* **1994**, *179*, 385–394.
- (40) Carnell, M.; Peyerimhoff, S. Ab initio investigation of the circular dichroism spectra of methylthiirane and trans-2, 3-dimethylthiirane. *Chem. Phys.* **1994**, *183*, 37–44.
- (41) Diedrich, C.; Grimme, S. Systematic Investigation of Modern Quantum Chemical Methods to Predict Electronic Circular Dichroism Spectra. *J. Phys. Chem. A* **2003**, *107*, 2524–2539.
- (42) Olsen, J. M.; Aidas, K.; Kongsted, J. Excited States in Solution through Polarizable Embedding. *J. Chem. Theory Comput.* **2010**, *6*, 3721–3734.
- (43) Olsen, J. M. H.; Kongsted, J. *Advances in Quantum Chemistry*; Elsevier, 2011; pp 107–143.
- (44) Sneskov, K.; Schwabe, T.; Kongsted, J.; Christiansen, O. The polarizable embedding coupled cluster method. *J. Chem. Phys.* **2011**, *134*, 104108.
- (45) Schwabe, T.; Sneskov, K.; Olsen, J. M. H.; Kongsted, J.; Christiansen, O.; Hättig, C. PERI-CC2: A Polarizable Embedded RI-CC2 Method. *J. Chem. Theory Comput.* **2012**, *8*, 3274–3283.
- (46) Hedegård, E. D.; List, N. H.; Jensen, H. J. A.; Kongsted, J. The multi-configuration self-consistent field method within a polarizable embedded framework. *J. Chem. Phys.* **2013**, *139*, 044101.

- (47) Hedegård, E. D.; Olsen, J. M. H.; Knecht, S.; Kongsted, J.; Jensen, H. J. A. Polarizable embedding with a multiconfiguration short-range density functional theory linear response method. *J. Chem. Phys.* **2015**, *142*, 114113.
- (48) Eriksen, J. J.; Sauer, S. P. A.; Mikkelsen, K. V.; Jensen, H. J. A.; Kongsted, J. On the importance of excited state dynamic response electron correlation in polarizable embedding methods. *J. Comp. Chem.* **2012**, *33*, 2012–2022.
- (49) Pedersen, M. N.; Hedegård, E. D.; Olsen, J. M. H.; Kauczor, J.; Norman, P.; Kongsted, J. Damped Response Theory in Combination with Polarizable Environments: The Polarizable Embedding Complex Polarization Propagator Method. *J. Chem. Theory Comput.* **2014**, *10*, 1164–1171.
- (50) Olsen, J.; Jørgensen, P. Linear and nonlinear response functions for an exact state and for an MCSCF state. *J. Chem. Phys.* **1985**, *82*, 3235.
- (51) Helgaker, T.; Coriani, S.; Jørgensen, P.; Kristensen, K.; Olsen, J.; Ruud, K. Recent Advances in Wave Function-Based Methods of Molecular-Property Calculations. *Chem. Rev.* **2012**, *112*, 543–631.
- (52) Helgaker, T.; Jørgensen, P. An electronic Hamiltonian for origin independent calculations of magnetic properties. *J. Chem. Phys.* **1991**, *95*, 2595–2601.
- (53) Cheeseman, J. R.; Frisch, M. J.; Devlin, F. J.; Stephens, P. J. Hartree-Fock and Density Functional Theory ab Initio Calculation of Optical Rotation Using GIAOs: Basis Set Dependence. *J. Phys. Chem. A* **2000**, *104*, 1039–1046.
- (54) Stephens, P. J.; Devlin, F. J.; Cheeseman, J. R.; Frisch, M. J. Calculation of Optical Rotation Using Density Functional Theory. *J. Phys. Chem. A* **2001**, *105*, 5356–5371.
- (55) Kongsted, J.; Nielsen, C. B.; Mikkelsen, K. V.; Christiansen, O.; Ruud, K. Nuclear

- magnetic shielding constants of liquid water: Insights from hybrid quantum mechanics/molecular mechanics models. *J. Chem. Phys.* **2007**, *126*, 034510.
- (56) Stephens, P. J.; Harada, N. ECD cotton effect approximated by the Gaussian curve and other methods. *Chirality* **2009**, 229–233.
- (57) Thellamurege, N. M.; Li, H. Note: FixSol solvation model and FIXPVA2 tessellation scheme. *J. Chem. Phys.* **2012**, *137*, 246101.
- (58) Nørby, M. S.; Steinmann, C.; Olsen, J. M. H.; Li, H.; Kongsted, J. Computational Approach for Studying Optical Properties of DNA Systems in Solution. *J. Chem. Theory Comput.* **2016**, *12*, 5050–5057.
- (59) Klamt, A.; Schüürmann, G. COSMO: a new approach to dielectric screening in solvents with explicit expressions for the screening energy and its gradient. *J. Chem. Soc., Perkin Trans. 2* **1993**, 799.
- (60) Stefanovich, E. V.; Truong, T. N. Optimized atomic radii for quantum dielectric continuum solvation models. *Chem. Phys. Lett.* **1995**, *244*, 65–74.
- (61) Truong, T. N.; Stefanovich, E. V. A new method for incorporating solvent effect into the classical, ab initio molecular orbital and density functional theory frameworks for arbitrary shape cavity. *Chem. Phys. Lett.* **1995**, *240*, 253–260.
- (62) Barone, V.; Cossi, M. Quantum Calculation of Molecular Energies and Energy Gradients in Solution by a Conductor Solvent Model. *J. Phys. Chem. A* **1998**, *102*, 1995–2001.
- (63) Klamt, A. Conductor-like Screening Model for Real Solvents: A New Approach to the Quantitative Calculation of Solvation Phenomena. *J. Chem. Phys.* **1995**, *99*, 2224–2235.
- (64) Cossi, M.; Barone, V. Analytical second derivatives of the free energy in solution by polarizable continuum models. *J. Chem. Phys.* **1998**, *109*, 6246–6254.

- (65) Aidas, K.; Angeli, C.; Bak, K. L.; Bakken, V.; Bast, R.; Boman, L.; Christiansen, O.; Cimiraglia, R.; Coriani, S.; Dahle, P.; Dalskov, E. K.; Ekström, U.; Enevoldsen, T.; Eriksen, J. J.; Ettenhuber, P.; Fernández, B.; Ferrighi, L.; Fliegl, H.; Frediani, L.; Hald, K.; Halkier, A.; Hättig, C.; Heiberg, H.; Helgaker, T.; Hennum, A. C.; Hettema, H.; Hjertenaes, E.; Høst, S.; Høyvik, I.-M.; Iozzi, M. F.; Jansík, B.; Jensen, H. J. A.; Jonsson, D.; Jørgensen, P.; Kauczor, J.; Kirpekar, S.; Kjaergaard, T.; Kloppe, W.; Knecht, S.; Kobayashi, R.; Koch, H.; Kongsted, J.; Krapp, A.; Kristensen, K.; Ligabue, A.; Lutnaes, O. B.; Melo, J. I.; Mikkelsen, K. V.; Myhre, R. H.; Neiss, C.; Nielsen, C. B.; Norman, P.; Olsen, J.; Olsen, J. M. H.; Osted, A.; Packer, M. J.; Pawłowski, F.; Pedersen, T. B.; Provasi, P. F.; Reine, S.; Rinkevicius, Z.; Ruden, T. A.; Ruud, K.; Rybkin, V. V.; Sałek, P.; Samson, C. C. M.; de Merás, A. S.; Saue, T.; Sauer, S. P. A.; Schimmelpfennig, B.; Sneskov, K.; Steindal, A. H.; Sylvester-Hvid, K. O.; Taylor, P. R.; Teale, A. M.; Tellgren, E. I.; Tew, D. P.; Thorvaldsen, A. J.; Thøgersen, L.; Vahtras, O.; Watson, M. A.; Wilson, D. J. D.; Ziolkowski, M.; Ågren, H. The Dalton quantum chemistry program system. *Wiley Interdisciplinary Reviews: Computational Molecular Science* **2013**, *4*, 269–284.
- (66) Olsen, J. M. H. PELib: The Polarizable Embedding library (development version). 2014.
- (67) Gao, B. Gen1Int Version 0.3.0. 2014; <http://repo.ctcc.no/projects/gen1int>.
- (68) Gao, B.; Thorvaldsen, A. J.; Ruud, K. Gen1Int: a unified procedure for the evaluation of one-electron integrals over Gaussian basis functions and their geometric derivatives. *Int. J. Quantum Chem.* **2010**, *111*, 858–872.
- (69) Ruud, K.; Helgaker, T. Optical rotation studied by density-functional and coupled-cluster methods. *Chem. Phys. Lett.* **2002**, *352*, 533–539.
- (70) Gagliardi, L.; Lindh, R.; Karlström, G. Local properties of quantum chemical systems: The LoProp approach. *J. Chem. Phys.* **2004**, *121*, 4494.

- (71) Vahtras, O. LoProp for Dalton. 2014; <http://dx.doi.org/10.5281/zenodo.13276>.
- (72) Shivakumar, D.; Williams, J.; Wu, Y.; Damm, W.; Shelley, J.; Sherman, W. Prediction of Absolute Solvation Free Energies using Molecular Dynamics Free Energy Perturbation and the OPLS Force Field. *J. Chem. Theory Comput.* **2010**, *6*, 1509–1519.
- (73) Guo, Z.; Mohanty, U.; Noehre, J.; Sawyer, T. K.; Sherman, W.; Krilov, G. Probing the alpha-Helical Structural Stability of Stapled p53 Peptides: Molecular Dynamics Simulations and Analysis. *Chemical Biology & Drug Design* **2010**, *75*, 348–359.
- (74) Bowers, K. J.; Sacerdoti, F. D.; Salmon, J. K.; Shan, Y.; Shaw, D. E.; Chow, E.; Xu, H.; Dror, R. O.; Eastwood, M. P.; Gregersen, B. A.; Klepeis, J. L.; Kolossvary, I.; Moraes, M. A. Molecular dynamics—Scalable algorithms for molecular dynamics simulations on commodity clusters. Proceedings of the 2006 ACM/IEEE conference on Supercomputing - SC 06. 2006.
- (75) Maestro version 2016-2. Schrödinger, LLC, New York, NY, 2016.
- (76) Jorgensen, W. L. Quantum and statistical mechanical studies of liquids. 10. Transferable intermolecular potential functions for water, alcohols, and ethers. Application to liquid water. *J. Am. Chem. Soc.* **1981**, *103*, 335–340.
- (77) Jorgensen, W. L.; Chandrasekhar, J.; Madura, J. D.; Impey, R. W.; Klein, M. L. Comparison of simple potential functions for simulating liquid water. *J. Chem. Phys.* **1983**, *79*, 926–935.
- (78) Yanai, T.; Tew, D. P.; Handy, N. C. A new hybrid exchange–correlation functional using the Coulomb-attenuating method (CAM-B3LYP). *Chem. Phys. Lett.* **2004**, *393*, 51–57.
- (79) Hariharan, P. C.; Pople, J. A. The influence of polarization functions on molecular orbital hydrogenation energies. *Theor. Chim. Acta* **1973**, *28*, 213–222.

- (80) Hehre, W. J.; Ditchfield, R.; Pople, J. A. *J. Chem. Phys.* **1972**, *56*, 2257–2261.
- (81) Francel, M. M.; Pietro, W. J.; Hehre, W. J.; Binkley, J. S.; Gordon, M. S.; DeFrees, D. J.; Pople, J. A. *J. Chem. Phys.* **1982**, *77*, 3654–3665.
- (82) Clark, T.; Chandrasekhar, J.; Spitznagel, G. W.; Schleyer, P. *J. Comput. Chem.* **1983**, *4*, 294–301.
- (83) Case, D. A.; Betz, R.; Cerutti, D. S.; Cheatham, T. E.; III.; Darden, T. A.; Duke, R. E.; Giese, T. J.; Gohlke, H.; Goetz, A. W.; Homeyer, N.; Izadi, S.; Janowski, P.; Kaus, J.; Kovalenko, A.; Lee, T. S.; LeGrand, S.; Li, P.; Lin, C.; Luchko, T.; Luo, R.; Madej, B.; Mermelstein, D.; Merz, K. M.; Monard, G.; Nguyen, H.; Nguyen, H. T.; Omelyan, I.; Onufriev, A.; Roe, D.; Roitberg, A.; Sagui, C.; Simmerling, C. L.; Botello-Smith, W. M.; Swails, J.; Walker, R. C.; Wang, J.; Wolf, R. M.; Wu, X.; Xiao, L.; Kollman, P. A. AMBER 2016. *University of California, San Francisco*. **2016**,
- (84) Korth, M. Third-Generation Hydrogen-Bonding Corrections for Semiempirical QM Methods and Force Fields. *J. Chem. Theory Comput.* **2010**, *6*, 3808–3816.
- (85) Nikitin, A. M.; Lyubartsev, A. P. New six-site acetonitrile model for simulations of liquid acetonitrile and its aqueous mixtures. *J. Comput. Chem.* **2007**, *28*, 2020–2026.
- (86) Becke, A. D. Density-Functional Thermochemistry. III. The Role of Exact Exchange. *J. Chem. Phys.* **1993**, *98*, 5648–5652.
- (87) Vosko, S. H.; Wilk, L.; Nusair, M. Accurate Spin-Dependent Electron Liquid Correlation Energies for Local Spin Density Calculations: a Critical Analysis. *Can. J. Phys.* **1980**, *58*, 1200–1211.
- (88) Lee, C.; Yang, W.; Parr, R. G. Development of the Colle-Salvetti Correlation-Energy Formula Into a Functional of the Electron Density. *Phys. Rev. B* **1988**, *37*, 785–789.

- (89) Jensen, F. Unifying General and Segmented Contracted Basis Sets. Segmented Polarization Consistent Basis Sets. *J. Chem. Theory Comput.* **2014**, *10*, 1074–1085.
- (90) Kendall, R. A.; Dunning, T. H.; Harrison, R. J. Electron affinities of the first-row atoms revisited. Systematic basis sets and wave functions. *J. Chem. Phys.* **1992**, *96*, 6796–6806.
- (91) Ufimtsev, I. S.; Luehr, N.; Martinez, T. J. Charge Transfer and Polarization in Solvated Proteins from Ab Initio Molecular Dynamics. *J. Phys. Chem. Lett.* **2011**, *2*, 1789–1793.
- (92) Bernasconi, L.; Sprik, M.; Hutter, J. Time dependent density functional theory study of charge-transfer and intramolecular electronic excitations in acetone–water systems. *J. Chem. Phys.* **2003**, *119*, 12417–12431.
- (93) Lever, G.; Cole, D. J.; Hine, N. D. M.; Haynes, P. D.; Payne, M. C. Electrostatic considerations affecting the calculated HOMO–LUMO gap in protein molecules. *Journal of Physics: Condensed Matter* **2013**, *25*, 152101.
- (94) Hopmann, K. H.; Ruud, K.; Pecul, M.; Kudelski, A.; Dračinský, M.; Bouř, P. Explicit versus Implicit Solvent Modeling of Raman Optical Activity Spectra. *J. Phys. Chem. B* **2011**, *115*, 4128–4137.
- (95) Štěpánek, P.; Bouř, P. Multi-scale modeling of electronic spectra of three aromatic amino acids: importance of conformational averaging and explicit solute–solvent interactions. *Phys. Chem. Chem. Phys.* **2014**, *16*, 20639–20649.
- (96) Olsen, J. M.; Aidas, K.; Mikkelsen, K. V.; Kongsted, J. Solvatochromic Shifts in Uracil: A Combined MD-QM/MM Study. *J. Chem. Theory Comput.* **2010**, *6*, 249–256.

## Supporting Information Available

Additional computational details regarding the setup of the molecular dynamics simulation



for the four stereoisomers of terrein. DALTON input and output along with relevant files for the project are available on Figshare (url: [https://figshare.com/projects/Modeling\\_electronic\\_circular\\_dichroism\\_within\\_the\\_Polarizable\\_Embedding\\_approach/20747](https://figshare.com/projects/Modeling_electronic_circular_dichroism_within_the_Polarizable_Embedding_approach/20747))

This material is available free of charge via the Internet at <http://pubs.acs.org/>.